Nonlinear Scattering and Trapping by Local Photonic Potentials

Y. Linzon,[1] R. Morandotti,[2] M. Volatier,[3] V. Aimez,[3] R. Ares,[3] and S. Bar-Ad[1]

[1]*School of Physics and Astronomy, Faculty of Exact Sciences, Tel-Aviv University, Tel Aviv 69978, Israel*
[2]*Universite' du Quebec, Institute National de la Recherche Scientifique, Varennes, Quebec J3X 1S2, Canada*
[3]*Centre de Recherche en Nanofabrication et en Nanocaracterisation (CRN), Universite de Sherbrooke, 2500 Boulevard Universite, Sherbrooke, Quebec, J1K 2R1, Canada*

(Received 20 December 2006; published 27 September 2007)

We experimentally study the nonlinear scattering by local photonic structures embedded in continuous Kerr media and demonstrate nonlinear trapping in guiding structures and resonant transmission in antiguiding structures. An intuitive physical picture is presented and verified in simulations.

DOI: 10.1103/PhysRevLett.99.133901 PACS numbers: 42.65.Sf, 42.25.Fx, 42.65.Jx, 42.81.Dp

Scattering by local potential discontinuities is a fundamental aspect of wave physics [1]. The most basic configuration is wave scattering in one dimension (1D), where there is a clear distinction between bound states, which exist only for attractive potential discontinuities, and continuum states, which are common to all geometries. Importantly, all states are orthogonal in the linear-wave regime. In particular, an excitation in the continuum is partially reflected and partially transmitted, but does not couple to a bound state. A well-known realization of 1D scattering involves the propagation of electromagnetic waves in planar waveguide structures. In this case, the photonic potential is a variation of the refractive index as a function of the x coordinate, which does not depend on the z coordinate. The z axis is then analogous to time in the scattering problem, and a decrease of the propagation constant β (the z-component of the wave number) corresponds to an increase of energy of a particle incident on the time-independent 1D potential. Here, the bound states are guided modes (which can only be excited by direct-coupling), and the continuum, scattering states are radiation modes (which can be excited by side-coupling, i.e., by a beam that enters the structure from the side, via the surrounding clad). Similarly to the scattering problem, the guided modes and radiation modes are completely decoupled in the linear regime. The analogy between the linear problems is well established. However, when the dielectric medium in which the wave propagates has a (Kerr-type) nonlinear response, the beam may effectively induce potential changes by itself, which would alter the scattering dynamics and lead to novel effects that are inhibited for linear waves and which have no known counterparts in the particle scattering problem. One possibility is a transfer of energy between orthogonal linear modes and, in particular, trapping of light by guided modes of the structure.

Experiments on nonlinearity-induced localization and trapping have been performed mainly on periodic waveguide arrays, which are 1D photonic crystals (PC). The interest in these systems arises from the fact that they exhibit a unique interplay between discreteness and nonlinearity, leading, for example, to the formation of discrete solitons [2,3]. Most of the research dealing with nonlinear scattering by PC has concentrated on local defects that are physically added to, or optically induced in, PC which are either infinite [4–7] or semi-infinite [8–10]. Localization of excitations belonging to band gaps in the linear spectra of PC has also been demonstrated, as gap solitons [11]. The common denominator of these works is that they deal with localized nonlinear excitations that penetrate into a gap of the linear spectrum of a periodic structure. In this Letter, however, we focus on a more fundamental problem, namely, scattering from a local, isolated structure embedded in a homogeneous continuum. This case has only been studied numerically [12–17]. We present (for the first time to the best of our knowledge) a detailed experimental study of nonlinear scattering by both guiding and antiguiding local potentials. In particular, we demonstrate nonlinear trapping in the guiding geometry. In contrast with earlier experiments, the nonlinearity-induced trapping that we observe is into an existing eigenmode of the linear system.

In the following, we give a simple and intuitive physical picture of the nonlinear trapping mechanism. The top part of Fig. 1 illustrates the linear scattering dynamics from a guiding scattering center (GSC), equivalent to a potential well, and from an antiguiding scattering center (AGSC), equivalent to a potential barrier [panels (a) and (b), respectively]. In both cases, a wave packet with a central transverse wave number k_x is incident from the left (a cladding with refractive index n_{clad}) on the scattering center (a core with n_{core}). Both structures resemble resonant cavities: the side-coupled power inside is transient and leaves as transmitted and reflected waves after a few cavity oscillations. Therefore, as $z \rightarrow \infty$, no power remains inside, and $R + T = 1$ (R and T being the reflection and transmission coefficients, respectively). The linear scattering may be represented in terms of plane wave transmission spectra $T(\beta)$, also shown in Figs. 1(a) and 1(b). With the total wave number $k = k_0 n_{\mathrm{clad}} = \sqrt{\beta^2 + k_x^2}$, where k_0 is the free-space wave number, a side-coupled excitation travelling with a tilt angle of θ has $\beta = k\cos\theta$ and $k_x = k\sin\theta$. Thus, an increase of the incidence angle pulls β deeper into the

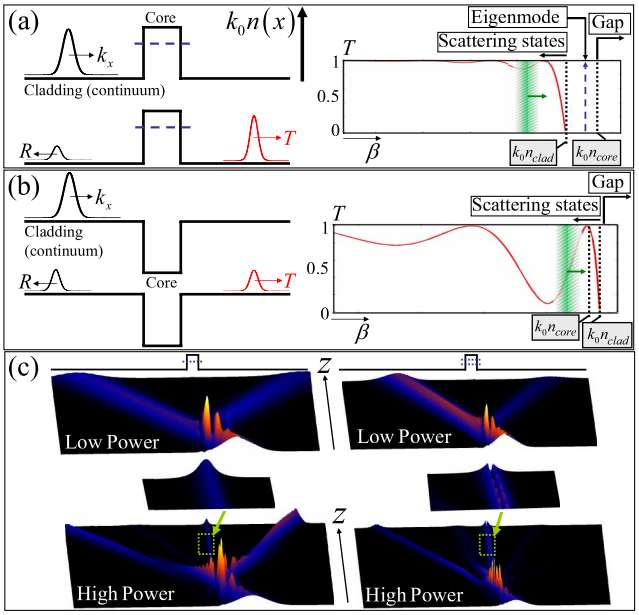

FIG. 1 (color online). (a,b) Scattering by (a) guiding and (b) antiguiding 1D centers. Incident, reflected, and transmitted wave packets are shown, as well as the confined eigenmodes of the guiding center and characteristic plane wave transmission spectra; the shaded bands illustrate the spatial frequency bands of wave packets, and the arrows indicate the nonlinearity-induced shift. (c) Simulations of linear scattering (top) and nonlinear trapping (bottom) in single-mode (left) and two-mode (right) 4 μm wide waveguides; the relative index steps are 0.3% and 0.7%, and the input angle is 3°.

scattering regime $\beta < k_0 n_{\text{clad}}$. Transmission resonances are observed in both GSCs and AGSCs for $\beta < k_0 n_{\text{core}}$, corresponding to constructive interference. Eigenstates, on the other hand, only exist in GSCs, in the interval $k_0 n_{\text{clad}} < \beta < k_0 n_{\text{core}}$, as indicated by the dashed vertical line in the corresponding transmission spectrum. The right hand side of each spectrum ($\beta > k_0 n_{\text{core}}$ for GSCs and $\beta > k_0 n_{\text{clad}}$ for AGSCs) constitutes a semi-infinite gap, in which no linear excitations exist. Finally, unlike monochromatic plane waves, incident wave packets have finite-width spatial frequency contents, shown as shaded vertical bands in the transmission spectra.

A focusing nonlinearity modifies the above picture. First, solitons may form in the semi-infinite gap [2]. In addition, when the GSC has more than one eigenmode, the nonlinearity can couple the directly-injected modes and induce energy exchange between them [18]. Turning back to the scattering problem, a moderate nonlinearity slightly modifies the transmission spectra [12–17], but its main effect can be regarded as follows: the effective wave number is now $\tilde{k}$, satisfying $\tilde{k}^2 \approx k_0^2(n_{\text{clad}}^2 + 2n_2 n_{\text{clad}} I)$, where n_2 is the Kerr coefficient and I is the power density of the wave packet. This shifts both k_x and β to higher values. Therefore, in the GSC geometry, it should become possible to shift some of the β components of a wave packet into bound states, in which they will trap. We note that a self-defocusing nonlinearity ($n_2 < 0$) cannot induce trapping, as it shifts β to lower values, away from the bound state, and also reduces the power density.

We first demonstrate such nonlinear trapping in numerical simulations of the 1D nonlinear Schrödinger equation, using the beam propagation method (BPM) [19], with parameters corresponding to silica glass [20]. Figure 1(c) shows scattering of low-power (top) and high-power (bottom) wave packets from a single-mode (left) and a two-mode (right) GSC. In the two-mode case the trapped power distribution is that of the waveguide's second linear mode, which has the lower β value and is therefore the first to be accessible to the wave packet as it shifts due to the nonlinearity. The trapped waves are numerically stationary for long propagation distances, and their shapes are identical to those of the directly-coupled linear eigenmodes (not shown). The latter demonstrates that the trapping is indeed into a linear mode rather than being a nonlinear localization. We note that the shape of the wave packet at the interface of the localized structure is critical, as the power density at the interface must be sufficiently high. An approximate condition for trapping into the eigenmode is $n_2 I \gtrsim |n_{\text{core}} - n_{\text{clad}}|$, with I itself being a dynamical variable, strongly dependent on the nonlinearity and the initial conditions. Finally, trapping was not observed in numerical simulations with a self-defocusing nonlinearity.

To experimentally test the above ideas, two different waveguide geometries were used as implementation of GSCs and AGSCs. Figure 2(a) shows 4 uncoupled GeB-doped single-mode silica glass (SiO_2) optical channels, each of 4×4 $(\mu\text{m})^2$ rectangular cross section, with 16 μm separation, embedded inside a 3 mm-wide pure silica glass (without a top clad). The compositions and optical properties of the layers are as in Ref. [20]. The four isolated waveguides, surrounded by glass of lower refractive index, form a local GSC for side-coupled excitations. Figure 2(b) shows a 3-layer $Al_xGa_{1-x}As$ sample, in which the middle, 1.5 μm-thick layer is of higher refractive index ($x = 0.18$) and serves as a planar waveguide core. The top, 1.5 μm-thick cladding layer ($x = 0.24$) is locally thinned to 0.1 μm by chemical etching, to effectively decrease the refractive index at the core layer relative to the surrounding (4 mm-wide) continuum (for details see

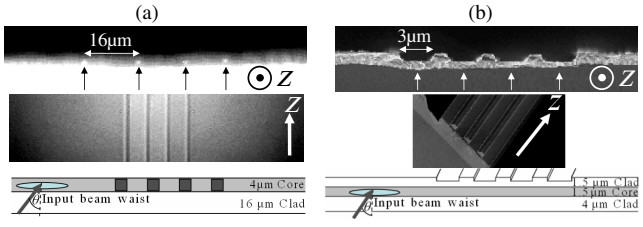

FIG. 2 (color online). Side views, top views, and cross-sections of the samples: (a) A silica sample (optical microscope images); (b) An AlGaAs sample (scanning electron microscope images). Arrows indicate the waveguide and antiwaveguide positions.

Ref. [3]). This produces 4 antiwaveguides, 3 μm wide and with 2 μm separations, serving as a local AGSC. In both types of samples, the guiding layer is a single-mode waveguide in the confined vertical direction, resulting in effectively 1D dynamics. Also note that the thicker parts of the AlGaAs sample have a higher effective refractive index, and therefore this sample does not support true guided modes (i.e., light which is directly coupled into the structure would ultimately tunnel out). An elliptical input beam, with an adjustable horizontal waist size and a vertical waist size that matches the samples' core thickness (see Fig. 2), is side-coupled into the continuum and directed towards the structure with a steerable input angle. A second beam, at normal incidence, is used for direct-coupling, as a means of identifying the waveguides' positions and for characterization of the linear modal shapes in the GSC. A few samples with identical cross sections and different lengths were used in each geometry, to characterize the output beam as a function of the propagation distance. In all measurements, the excitation is by 80-fs laser pulses at a 1 kHz repetition-rate (Spectra Physics OPA), yielding up to 20 MW peak power at a wavelength of $\lambda_0 = 1520$ nm, where both silica and AlGaAs are transparent and exhibit a focusing Kerr nonlinearity. When this beam is coupled to the continuum, far away from the local structures, spatial solitons are formed in this power range.

Experimental results are shown in Fig. 3 for the GSC geometry and in Fig. 4 for the AGSC geometry. In most of our measurements, a 40 μm-wide input beam was used, which is comparable to the total widths of the scattering centers and an order of magnitude larger than the individual scatterers. This beam size yields sufficient angular resolution in the scattering experiments and simplifies the coupling into the sample. Scans of the output facet as a function of the input tilt angle, for low-power excitation of an 8 mm-long sample [Fig. 3(a)], reveal the first transmission resonance, and show that only a negligible fraction of the power emerges from the waveguide positions. As the peak power is increased to levels in which the nonlinearity-induced index variation $n_2 I$ is comparable to $n_{\text{core}} - n_{\text{clad}}$ [Fig. 3(b)], the output beam is more focused, and at large tilt angles, it is emerges outside the field of view of the imaging camera. More importantly, the power fraction that emerges from the first waveguide increases dramatically at the angle interval 3–6°. The output intensity distributions coincide with the linear modal shape. This suggests a nonlinearity-induced trapping of power in the GSC. To confirm this hypothesis, we repeated the measurement with a 28 mm-long sample, excited under identical conditions [Fig. 3(c)]. This measurement also shows a substantial power fraction inside the first waveguide, in the same angle interval. The fact that power is found in the waveguide in the same angle interval for both samples, although the propagation lengths are substantially different (by a factor of 3.5), suggests that power is indeed trapped in the waveguide. At the same time, the fact that only a fraction of the power is trapped (up to 20%) suggests that

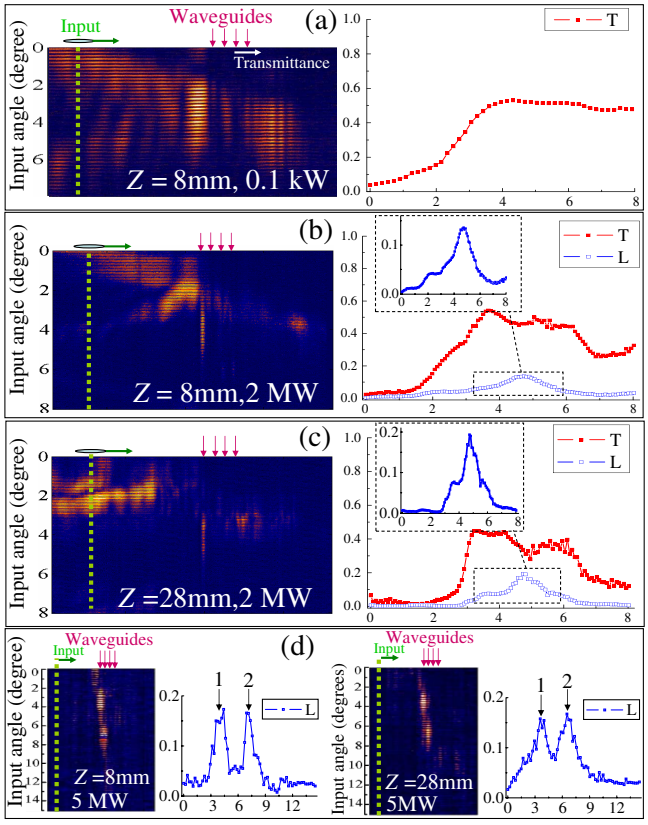

FIG. 3 (color online). Scattering in the silica samples. The left panels in (a)–(c) show output intensity profiles as a function of the input angle for a 40 μm-wide input beam. The dashed lines and arrows indicate the input and waveguide positions, respectively; the right panels and insets show the transmitted (T) and trapped (L) power fractions, and L on a magnified scale. Sample lengths and excitation peak powers are indicated; (d) Data for a 150 μm-wide input beam.

the resulting excitation may be either linear (for low trapped power) or nonlinear (for high trapped power). Figure 3(d) shows results of nonlinear trapping in the two samples, with a 150 μm-wide input. Trapping in the first waveguide is observed at the angle interval 3–5°, and in the second waveguide at the angle interval 6–8°, for both samples. The clear angular distinction between trapping in the first and second waveguides in this measurement results from the higher angular resolution obtained with the wider input beam (i.e., due to the narrower spatial frequency content of the input beam).

With the AlGaAs samples, shorter propagation lengths and lower input powers were used, on account of temporal dispersion, the higher Kerr coefficient, and lower damage threshold. A 40 μm-wide input beam was used, and the input intensity was again adjusted to match the nonlinearity to the refractive index variations. Scans of the output facet as a function of the incidence angle for a 3 mm-long sample [Fig. 4(a)] show a substantial amount of power emerging from the AGSC for the angle interval 2–6°. However, in the case of a 4.2 mm-long sample, with

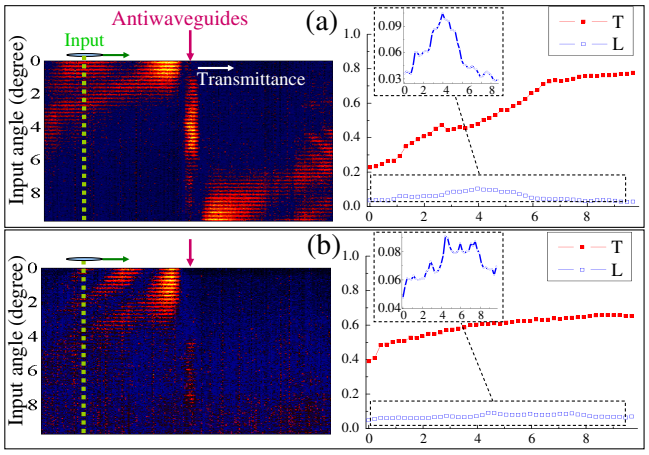

FIG. 4 (color online). Scattering in (a) 3 mm and (b) 4.2 mm-long AlGaAs samples, excited by a 40 μm-wide, 1 kW input beam. The panel contents are arranged as in Figs. 3.

identical excitation conditions [Fig. 4(b)], the AGSC is virtually empty in the same angle interval. In parallel, the transmitted power fraction in the same angle interval increases. Thus, we conclude that there is no trapping in this case, but only transient cavity oscillations.

Simulations of scattering from the actual, multisite centers confirm the experimental results. When a high-power input beam is launched towards the 4-site GSC, nonlinear trapping in the first and second sites is observed in different input angle intervals [Figs. 5(a) and 5(b), respectively]. Narrower input beams result in narrower trapping angle intervals and in reduced trapped power fractions. Simulations for the 4-site AGSCs do not exhibit nonlinear trapping. In agreement with the data in Fig. 4, power found in the AGSC's resonator-like structure at certain angle intervals for short propagation distances [Fig. 5(c)] exits the structure after a slightly longer propagation distance [Fig. 5(d)].

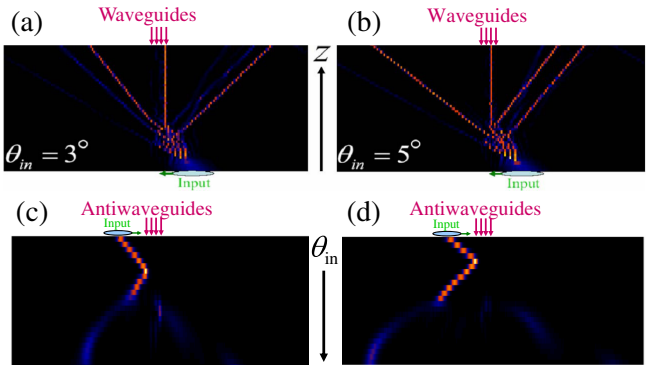

FIG. 5 (color online). (a) and (b) Simulations of trapping in a 4-site GSC, with parameters corresponding to silica, a 100 μm-wide, 4 MW (peak) input beam, and input angles of (a) 3° and (b) 5°. (c) and (d) Simulations of nonlinear scattering from a 4-site silica AGSC, as a function of input angle, following propagation of (c) 4.1 mm and (d) 5.8 mm.

In summary, we have studied experimentally and numerically the nonlinear scattering of electromagnetic guided waves by local photonic potentials and report the first observation of nonlinear trapping into the linear modes of guiding scatterers. Selective trapping of wide input beams to individual constituent sites in the scattering from multisite guiding centers has been demonstrated experimentally and numerically. The higher linear modes of multimode scatterers can be excited with appropriate experimental conditions [Fig. 1(c)], suggesting a unique way to selectively excite the higher modes of a confined structure. While an intensity-controlled waveguide selection, at a given tilt angle, was not observed, it may become possible with an appropriate sample design, and would be of interest for nonlinear switching applications. Finally, similar phenomena should also be observed in other realizations of wave scattering by local attractive and repulsive potentials, for example, in the nonlinear scattering of matter-wave Bose-Einstein condensates from localized optical potentials.

This work was supported by ISF Grant Nos. 8006/03 and 944/05, and by NSERC in Canada. We are grateful to V. Fleurov and A. Gorbach for enlightening discussions.

[1] See, e.g., J. D. Jackson, *Classical Electrodynamics* (J. Wiley and Sons, New York, 1998), 3rd ed., Chap. 10; E. Merzbacher, *Quantum Mechanics* (J. Wiley and Sons, New York, 1961), Chap. 6.
[2] D. N. Christodoulides and R. I. Joseph, Opt. Lett. **13**, 794 (1988); D. N. Christodoulides and E. D. Eugenieva, Phys. Rev. Lett. **87**, 233901 (2001).
[3] H. S. Eisenberg *et al.*, Phys. Rev. Lett. **81**, 3383 (1998).
[4] A. B. Aceves *et al.*, Phys. Rev. E **53**, 1172 (1996).
[5] W. Królikowski and Y. S. Kivshar, J. Opt. Soc. Am. B **13**, 876 (1996).
[6] R. Morandotti *et al.*, Opt. Lett. **28**, 834 (2003).
[7] L. Morales-Molina and R. A. Vicencio, Opt. Lett. **31**, 966 (2006).
[8] S. Suntsov *et al.*, Phys. Rev. Lett. **96**, 063901 (2006).
[9] C. R. Rosberg *et al.*, Phys. Rev. Lett. **97**, 083901 (2006).
[10] K. G. Makris *et al.*, Opt. Lett. **31**, 2774 (2006).
[11] D. Mandelik *et al.*, Phys. Rev. Lett. **92**, 093904 (2004); O. Manela *et al.*, Opt. Lett. **29**, 2049 (2004).
[12] X. D. Cao and B. A. Malomed, Phys. Lett. A **206**, 177 (1995).
[13] H. Sakaguchi and M. Tamura, J. Phys. Soc. Jpn. **73**, 503 (2004).
[14] R. H. Goodman *et al.*, Physica D (Amsterdam) **192**, 215 (2004).
[15] B. Piette *et al.*, J. Phys. A **38**, 10403 (2005).
[16] A. E. Miroshnichenko *et al.*, Chaos **13**, 874 (2003).
[17] K. T. Stoychev *et al.*, Phys. Rev. E **70**, 066622 (2004).
[18] D. Mandelik *et al.*, Phys. Rev. Lett. **95**, 073902 (2005); A. Soffer and M. I. Weinstein, Phys. Rev. Lett. **95**, 213905 (2005).
[19] The BPM code is available at http://www.freeBPM.com.
[20] D. Cheskis *et al.*, Phys. Rev. Lett. **91**, 223901 (2003).